12-2007

Investigating hydrophilic channels in polymer composites using atomic force microscopy.

Matthew David Cummins
University of Louisville

INVESTIGATING HYDROPHILIC CHANNELS IN POLYMER COMPOSITES USING ATOMIC FORCE MICROSCOPY

By

Matthew David Cummins
B.S.CHE, University of Louisville, 2006

A Thesis
Submitted to the Faculty of the
University of Louisville
J. B. Speed School of Engineering
as Partial Fulfillment of the Requirements
for the Professional Degree

MASTER OF ENGINEERING

Department of Chemical Engineering

December 2007

INVESTIGATING HYDROPHILIC CHANNELS IN POLYMER COMPOSITES USING ATOMIC FORCE MICROSCOPY

Submitted by:_____
Matthew David Cummins

A Thesis Approved on

_____
(Date)

by the Following Reading and Examination Committee:

_____
Dr. Gerold Willing

_____
Dr. James Watters

_____
Dr. Andrea Knox-Kelecy

ACKNOWLEDGEMENTS

I would like to acknowledge Dr. Gerold Willing, my thesis advisor, for his help at each stage of the thesis process. I would like to thank Dr. Millicent Firestone and Argonne researchers for procuring the samples and providing the information necessary to complete this work. I would like to thank Dr. Watters and Dr. Kelecy for being on my defense committee and allowing me to graduate. Last but not least, I would like to acknowledge and thank my family and friends for there constant support and love.

ABSTRACT

Nanoscience is not about products becoming smaller and smaller, but about new material properties being exploited for new and enhanced product applications. Liquid crystalline materials are one branch of "nanomaterials" that has promise of highly useful products. Liquid crystalline materials are soft materials that can respond to external stimuli and form ordered structures. Liquid crystals have applications as templates for more complex nanostructures as well as sensing devices. The purpose of this study was to investigate, using atomic force microscopy, the characteristics of a liquid crystalline, nanoparticle, composite material to determine whether or not it was indeed forming ordered, hydrophilic channels lined with gold nanoparticles. Atomic force microscopy showed that these channels were indeed forming, but further investigation will be necessary before the structures could be controlled and exploited.

TABLE OF CONTENTS

LIST OF FIGURES

I. INTRODUCTION

With the growth of nanoscience in the 21st century and electronic devices becoming smaller and smaller, the development of new materials, which address the needs of the new technologies, will become ever more necessary. The development of "soft materials" or liquid crystals is a major contribution to the increasing demand for nanoscale building blocks for new technologies. There is a focused drive towards the development of self assembling materials that can be externally controlled with an eye to the production of sensing devices, nanostructure building blocks, and other optical, thermal or electrical property based applications. Self assembling materials are materials that can change chemical or physical properties as a result of external stimuli. Ionic liquids (ILs) are one particular type of self assembling material in which the ionic properties of particular materials are used to develop stable, self-assembled structures that can be used for various applications. In this particular investigation, an ionic liquid polymerization reaction was conducted with a nanoparticle precursor and atomic force microscopy was used to determine the presence of ordered hydrophilic channels within the material.

A. Background: Soft Materials

The focus of nanoscience is on the development of materials that exhibit unique qualities that can be exploited for various applications. These chemical and electrical

properties are the result of high surface area to volume ratios and the confinement of electronic states of nanomaterials (Shenhar 2005). Liquid crystals, soft materials that can self-assemble into ordered structures, offer a wide range of opportunities for the development of advanced nanostructures (Kato 2006). The field of liquid crystal development is a relatively new and large field with many sub-divisions. However, the development of nanostructures within these liquid crystals is relatively new and has only been investigated by a few researchers (Hoshino 2003, Yoshizawa 2005). These nanoparticle-composite soft materials carry a number of exceptional properties that ensure their place in the ever growing nano-industry (Kato 2006). The composite used in this study is a great example. The specific ionic liquid crystal composite used was a 1-decyl-3-methylimidazolium chloride $[C_{10}mim^{+}][Cl^{-}]$ laced with gold nanoparticles. During polymerization, the polymer assembles to form liquid crystalline mesophases which can be tuned from a 1D lamellae to 2D hexagonal or 3D bicontinuous structures (Batra 2007). These structures can serve as templates for the generation of nanostructures within the polymer, in this case - linear channels lined with gold. The polymer swells on contact with ethanol causing the linear chains of gold particles to lose their ordered arrangement and enter into a non-ordered arrangement. This particular phenomenon could lead to applications for sensing equipment where the environment in which a material is placed can affect the conduction of electricity through the metal particles and function as a switch.

In addition to sensing applications, one very novel aspect of the development of this material is its simplicity. The entire development of the material takes place in a tube in which the ionic liquid, a polymerization initiator, a gold precursor, and water are

mixed and irradiated with UV light to form the nanoparticle-polymer composite. This method of development is much simpler than other methods used to develop soft material based nanostructures. Researchers have attempted development of composite nanostructures on solid surfaces (Adachi 2000), bimolecular and polymer scaffolds (Zehner 1998, Warner 2003, McMillan 2002, Shenhar 2005, Peceros 2005, Lee 2006), and at solution interfaces (Lin 2003). One author has written:

> "These approaches have yielded nanoparticle ensembles that possess novel physical properties with potential application in sensing, optical information processing, and magnetic data storage. While periodic order is widely regarded as the ultimate goal in producing self-assembled films, these films actually possess order only on a local level. Furthermore, they are often difficult to fabricate reproducibly and frequently lack adequate durability for practical utilization." (Batra 2007)

Because of the simplicity of production of the material and its dynamic, but controllable nature, the gold nanoparticle-polymer composite, and materials similar to it could turn out to be building blocks for more complex nanostructures or the major "manipulated variable" in sensing and control devices.

B. Development of the composite polymer

Previous work by Argonne researchers showed that N-alkylmethylimidazolium based ionic liquids (ILs) self assemble to form liquid crystalline mesophases (Batra 2007). These mesophases are the result of electrostatic forces in the headgroup of the polymer and weak van der Waals forces in the tail. The Argonne study also showed that the addition of water to 1-decyl-3-methylimidazolium chloride [C10mim+][Cl-] can enhance the self-organization of the polymer and initiate gelation. One very valuable aspect of these materials is that their structures can be chemically modified from 1D lamellae to 2D hexagonal or 3D bicontinuous structures with perforated lamellae and

hydrophilic channels. Figure 1 illustrates a bicontinuous structure with perforated lamellae and hydrophilic channels.

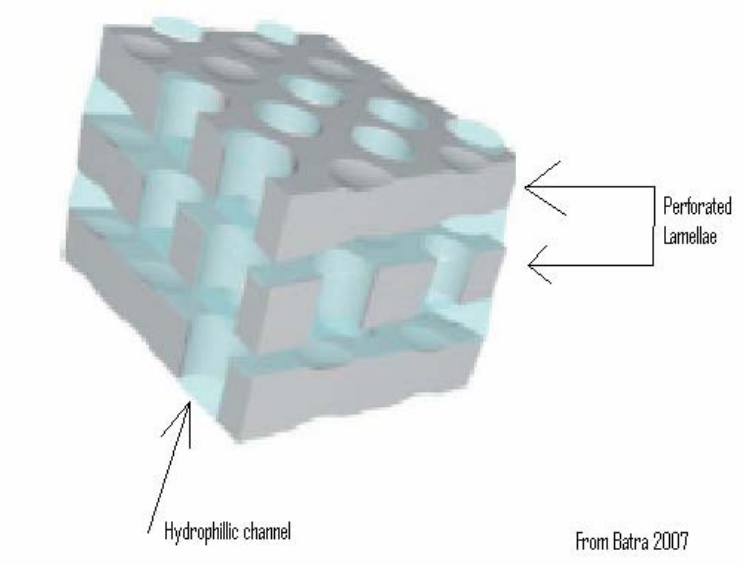

Figure 1- Schematic of a 3D bicontinuous structure

These structures can be used as templates for promoting the nucleation and growth of anisotropic gold nanoparticles. The materials used in this investigation were slightly modified to enhance the capacity of the material to form gold nanostructures. Regarding these modifications, Argonne researchers wrote:

> "The polymer used in this experiment was enhanced by introducing strong covalent interactions through polymerization at the cation headgroup by replacing the methyl group with a vinyl moiety. This does not interfere with the weak noncovalent interactions that promote the self assembly into well ordered structures. These modifications were made so as to retain the ability to spatially localize gold nanoparticles within defined hydrophilic compartments in the anisotropic matrix, while adding the property of programmed responsiveness (Batra 2007)."

There have been very few reports of polymerization reactions that have resulted in nanostructured components within the reaction itself (Hoshino 2003, Yoshizawa 2005).

The reaction of the polymer-particle composite begins with a mixture of 1-decyl-3-vinylimidazolium chloride $[C_{10}Vim^{+}][Cl^{-}]$ monomer and an aqueous solution of

$HAuCl_4$. Before the reaction takes place, the material is a homogenous, yellow, viscous liquid. The introduction of water initiates self-assembly into a liquid crystalline phase. The polymer-particle composite is photopolymerized under 400 Watts of UV irradiation for 1.5 to 2 hours, which converts the yellow liquid to a reddish-brown solid. This is consistent with the reduction of $AuCl_4^-$ to Au_0 (Batra 2007).

The $[C_{10}VIm^+][Cl^-]$ polymeric gel exhibits reversible swelling in aqueous and organic solvents, such as ethanol. When the polymeric sample is immersed in ethanol, the material swells, reaching a maximum swell size in about 3 hours at room temperature. When the polymer, under ambient conditions, is allowed to dry, it takes approximately 2 hours for the polymer to return to its initial pre-swollen size.

The change in mesostructure of the polymer was studied (Batra 2007) using small angle x-ray scattering (SAXS). The SAXS data showed that in the swollen state, the polymeric structure was disordered. As drying time increased, the polymer became more organized. The SAXS data revealed diffraction patterns consistent with a hexagonal mesostructure after approximately 2 hours of drying. TEM and energy-dispersive X-ray spectroscopy conducted on the polymer sample particles revealed that their size ranged from 10 to 40 nm and that their primary component is gold. Vis-Near Infrared (NIR) Spectroscopy was conducted to gather information about the morphology and packing arrangement of the ethanol swollen and dried samples. NIR spectroscopy revealed that as the polymer continued to collapse from drying the particles were assembling themselves in chain like structures within the polymer.

> "It is possible that such a nanoparticle organization may be driven by structural rearrangements in the polymer that occur during the loss of ethanol and contraction, that is, as the polymer structure evolves towards a more well-ordered, hexagonally perforated lamellae (de-swollen state), the nanoparticles may be

> driven to occupy the ordered columns of the hydrophyillic regions. Such an arrangement may drive the organization of the gold particles to pack into 1D chainlike configurations thereby enhancing interparticle coupling (Batra 2007)."

The purpose of the ensuing investigation is to find evidence for and confirm that gold nanoparticles are indeed forming chains in the hydrophilic regions of the hexagonally packed nanoparticle-composite polymer.

C. Equipment: Atomic Force Microscope

In order to determine whether or not the gold nanoparticles are forming chains through the hydrophilic regions of the hexagonally packed composite polymer, atomic force microscopy (AFM) was utilized to image the surface of the polymer. AFM has the advantage of obtaining a "real" image of the polymer as opposed to relying on x-ray and infrared beam diffraction angles, which only provide "projected images" of the particles in the polymer.

Atomic force microscopy is a method of developing images of a surface that utilizes a micron-scale cantilever, in this case a 125 μm long cantilever, which is sensitive to the atomic scale surface interaction forces, to scan over the contours of a surface and create an image. In AFM, the cantilever is brought to within a few hundred nanometers of a surface where it can detect the surface forces. The cantilever then swept back and forth across the surface in a linear path which develops a straight line contour of the surface. Once one contour line is drawn, the AFM will start a new contour line parallel to the previous one, a small distance away. This process continues until the desired area of scanning is completed. The contour lines are not drawn directly by the cantilever. A laser beam that is deflected off the back of the cantilever is received by a photodiode, which measures the deflection of the cantilever relative to an origin point on

the diode. For example, if a relatively flat surface has a 200 nm hill on it, the cantilever will pass along the flat surface and over the hill. The cantilever, when it passes over the hill, will deflect the laser in proportion to the height of the hill, and the photodiode will process the deviation in signal and plot the entire deflection along the hill with respect to position of the cantilever in its sweep. The summation of each "infinitesimal" deflection, including the flat surface preceding and proceeding the hill will be plotted as the contour line. With each incremental change of the cantilever in the x, y, or z direction an "image" of the surface is generated.

The advantage of AFM, in the context of this experiment, is that one can get an actual image of how the gold nanoparticles arrange themselves throughout the polymer, as opposed to making predictions based upon mathematical models and the diffraction of x-ray and infrared beams. However, there are a few drawbacks to using atomic force microscopy. First, AFM can only develop an image of a surface. Where x-ray and IR methods can actually make predictions about the structure of the polymer throughout an entire sample, AFM can only show the arrangement of particles and the structure of the polymer if certain features happen to be present in the area scanned. Another drawback to the use of AFM is that it relies heavily on chance. While one could predict where the particles will be on the polymer based upon the dark purple coloration at different regions of a sample, it is more difficult to tell whether one will see the end of a channel or a cross section of a channel when choosing a region to scan. If indeed the particles are arranging in the hydrophilic region of a hexagonally packed polymer, some areas scanned may be merely showing the tip of a channel, where one would only see a few particles, and other areas may show a cross-section of the longitudinal axis of a channel may be seen.

D. Objectives

The purpose of this investigation is to examine whether or not the nanoparticles are forming organized, controllable structures within the polymer. It is anticipated from previous work that the polymer composite is forming hydrophilic channels that are lined with gold nanoparticles. In this investigation, AFM was used to image these channels under various conditions in order to understand the conditions under which these structures are created. If the presence of these nanostructures is confirmed, it will have significant ramifications for the development of nanomaterials that can be used for sensing devices and other nano-product developments

II. CHARACTERISTICS OF COMPOSITE SAMPLES

The polymer composites were provided in microtomed, ethanol immersed samples, polymerized samples that were not yet immersed in ethanol, and ethanol immersed and dried samples cut for AFM imaging with a razor blade. Microtoming is a process of thinly slicing a material for applications like TEM imaging. Figure 2 shows the cylindrical composite just after polymerization prior to immersion in ethanol. It is in a cylindrical shape as a result of being polymerized in small capillary tubes. This particular tube sample is approximately 0.5 cm long and 0.08 cm in diameter. Careful inspection of the polymer in Figure 2 shows two differently colored regions extending down the length sample. From the angle at which the picture was taken, one can see a dark purple region and a beige colored region.

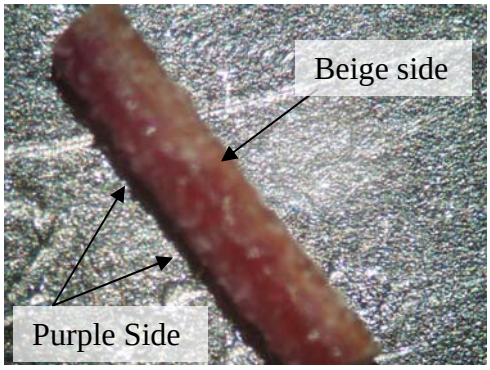

Figure 2 - Side view of gold-laced polymer

The reduction of the gold precursors to gold nanoparticles takes place during the polymerization reaction and turns the material to a dark purple shade in areas where these

particles are present. Therefore, the dark purple regions of the polymer represent regions where gold nanoparticles are present. The beige regions are simply polymer that is devoid of nanoparticles.

The angle of this particular image is somewhat deceptive, as the purpose of the image was to show nanoparticle regions. In actuality, the dark purple, gold nanoparticle laden region is actually a stripe that extends along the outer region of the polymer. The majority of the volume of the polymer is completely devoid of nanoparticles. As will be seen from the various cross-sections taken of the polymer, the gold nanoparticles are present along the outer ridge of the polymer, with no particles present towards the middle. This suggests that the nucleation of the particles tends to take place along the higher energy glass surface of the tube or that the UV light is not penetrating deeply into the sample.

Figure 3 is a digital camera image of the cross section of the composite as it would appear previous to ethanol immersion and just after polymerization. This image reveals a more accurate depiction of the distribution of the gold nanoparticles throughout the sample. On the left hand side of the cross section, one can see a dark purple region, which signifies the presence of gold nanoparticles. Away from the left hand ridge, through the center and all the way to the right hand side of the cross section, the predominant color is beige. The beige color is a region of the polymer that is devoid of nanoparticles. This picture clearly shows that the majority of the polymer is devoid of particles. Upon further AFM imaging, it was discovered that even some of the purple regions were deceptive in terms of the presence of particles. It was not until images were taken of the very edge regions of these particles that any significant concentration of

particles was shown. The highest concentration of particles were found, not along the interior ridges of the cross section, but along the “shell” or sides of the longer samples. This, once again, illustrates the idea that gold nanoparticle nucleation is either severely reliant on the presence of the high energy, bent, glass tube surface or that the UV radiation is only reaching one edge of the sample.

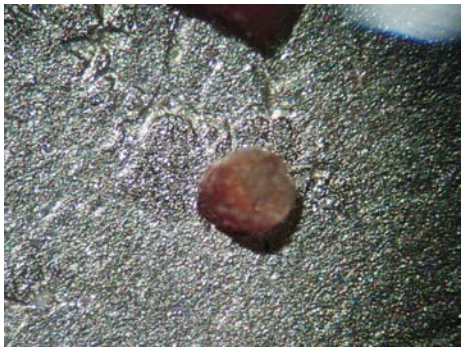

Figure 3 - Cross-Section of Gold-laced polymer (no ethanol applied)

III. DEVELOPMENT OF SAMPLES FOR AFM

To determine what sort of nanoparticle and polymeric structures were present in the polymer before and after ethanol immersion, careful consideration was taken in terms of the development of samples for AFM imaging. Multiple polymer composite samples were prepared by Argonne researchers and provided for AFM imaging. The ultramicrotomed TEM samples from a previous study (Batra 2007) were the first samples scanned. Samples previously soaked in ethanol and sliced with an ultrafine razor blade were also provided. The polymer composites examined in Figures 2 and 3 were also provided by Argonne and were initially a few centimeters long. These samples, as mentioned before, were not soaked in ethanol to enable comparisons between immersed and non-immersed samples. However, cross-sections were cut from the "non-immersed" samples and immersed in ethanol and dried to develop new "immersed" samples for examining the polymeric structures.

In order to scan these samples, the cylinders had to be sliced down to sizes that were appropriate for AFM imaging. It was imperative that the surfaces scanned be representative of the "untouched" cross section of the polymer. The purpose of this project is to examine the structures created by the polymer during self-assembly. Therefore, any modifications made to the surface after ethanol was dried from the surface would not be representative of these self-assembled structures. For instance any debris or

striations from slicing the polymer could affect the overall morphology of the surface, thereby creating an image that did not represent the actual structure constructed after ethanol drying.

A good example of how preparation of the polymer can detrimentally affect the AFM images produced is the sample in Figure 4, which was cut by common razor blades. Figure 4 is a cross section of the cylindrical polymer composite sample after being cut by a razor blade. The striations across the sample are obvious. Because of the nature of AFM imaging, it would be difficult to differentiate between channels formed by striations from a razor blade and channels formed as a result of polymeric self-assembly. The razor blades also tended to leave particulate debris within the striations they created. Once again, the nature of AFM imaging did not lend itself to differentiating between particle like debris formed as a result of razor blade cuts and nanoparticles formed during the reduction of the gold precursors.

Figure 4 – Cross section of striated sample

After it was determined that a common razor blade produced too many striations on the polymer to do an effective analysis of the material (Figure 4), other methods of developing samples from the non-immersed polymers were attempted. Freezing the polymer with liquid nitrogen and then snapping it in an attempt to produce a uniform surface for examining did not produce very useful results. Interestingly enough, the polymer, in an expanded ethanol absorbed phase, thawed very fast after being frozen. The thaw occurred fast enough that upon attempting to break the gel, it simply fell apart in the tweezers in which it was being held. Simply snapping the expanded, ethanol absorbed polymer was also attempted. This had similar results as the nitrogen attempt in that the gel tended to fall apart very easily. The most effective method, and most simple, was to snap the dry non-immersed polymeric cylinders using tweezers. Although the surfaces created were not uniformly flat in this method, there were enough flat regions in the developed cross section to enable AFM imaging. Some of the snapped samples were used for imaging directly and others were soaked with ethanol and dried, to further examine structural changes. Since the TEM, razor blade, and snapped samples were the only ones that yielded worthy images, the images generated from those samples will be used in discussing the results of the experiment. It is important to note here that each sample type was used to generate multiple samples. Therefore, the results described below are not unique to only one specific sample used in the AFM scans but are instead reproducible.

IV. METHODS AND MATERIALS

The samples examined in the rest of the thesis were of three kinds: ethanol immersed and dried microtomed TEM samples, dry non-immersed samples that were mechanically snapped to form cross sections, and ethanol immersed and dried samples cut with a very fine razor blade to form a cross section. The procedure for producing the TEM samples, which were used in SAXS analysis was described in a previous work (Batra 2007).

The dry, non-immersed, mechanically snapped samples were created from the composite material provided by Argonne National Laboratory. The composite material arrived in cylindrical pieces (a result of the capillary tubes in which they were polymerized) a few centimeters long. These samples were not processed at all after polymerization. To create cross sections for AFM imaging, the samples were simply held between two tweezers and mechanically bent to a breaking point to develop a cross-section for imaging. Because the material is very flexible, it was important to keep the tweezers holding the polymer very close together to ensure a clean break. Holding the tweezers at each end of the cylindrical polymer would allow too much bending and deformation of the polymer in trying to break it.

The dry, ethanol-immersed samples were created at Argonne. After polymerization, these samples were immersed in ethanol for approximately three hours

and then allowed to dry for another three hours to ensure that the polymer was fully swollen and fully contracted upon drying. Once the samples were dried, they were cut with a very fine razor blade that did not leave striations along the cross-section of the surface.

The atomic force microscope used in imaging these samples was a PSIA XE-100 instrument. The cantilevers used in scanning the surfaces were Applied Nanostructures (ACTA-10) aluminum coated, non-contact silicon cantilevers. The tips of these cantilevers ranged from 12-16 μm in height and had a radius of less than 10 nm.

The size ranges for all the images ranged from between 0.5 to 40 μm (ex. 40 μm x 40 μm) at 256 X 256 pixels. The scan rate, the speed at which the cantilever sweeps back and forth, was typically held between 0.2 and 0.4 Hz depending upon the area scanned. The cantilever was operated in non-contact mode at distances from the surface ranging between 20 and 150 nm.

V. TEM SAMPLES

The first AFM samples scanned were the microtomed samples used for TEM by Argonne Laboratories in a previous study on the polymer composites. When viewed under a microscope, the microtomed samples were a thin, transparent sheets. The TEM samples have the advantage of providing an extremely thin, mostly flat surface that is very conducive to AFM imaging. It was anticipated that particles present in the polymer at the surface of the TEM sheets could provide insight into the packing arrangement of the polymer and particles in the larger samples. Figure 5 is a screen shot of the cantilever scanning over the TEM sample. The copper grid structure in Figure 5 is the base upon which the microtomed sample was placed. The entire grid was fixed in a circular space approximately 0.5 cm in diameter. In Figure 5, the transparent microtomed sample can be seen as slight ripples due to diffracted light from the microscope and the AFM laser bouncing off the cantilever. The thin microtomed samples were conducive to AFM imaging because of the relatively smooth surface and relatively smooth contours. This is in severe contrast to the other samples which had very irregular contours and features that changed the height at which the cantilever scanned by orders of magnitude, making it difficult at times to find places to scan on the sample.

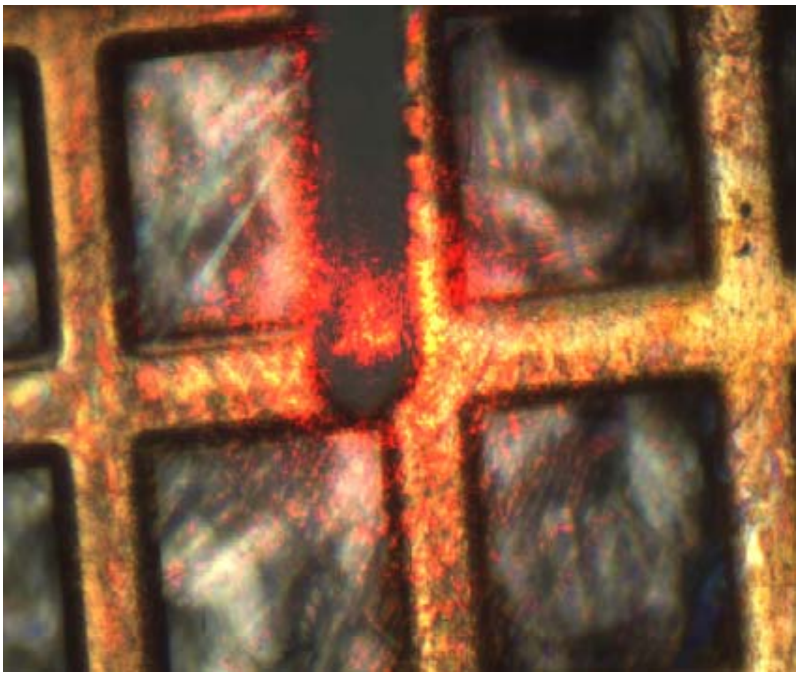

Figure 5 – Image of TEM sample taken during AFM scanning

Figures 6 through 11 were taken from multiple microtomed samples. The dark box in Figure 6 highlights a linear arrangement of particles on the polymeric surface. Figure 6 shows not only orderly arrangements of particles, but also very organized folds in the polymer itself. The lines seen running parallel to the particles are most likely the result of striations generated from microtoming the sample. The precise linearity of these lines suggests that they are the product of striations from mechanically cutting the sample rather than self-assembly from a polymer, which is likely to be much less linear. This concept will be further evidenced by images of actual channels taken from ethanol immersed sample cross sections.

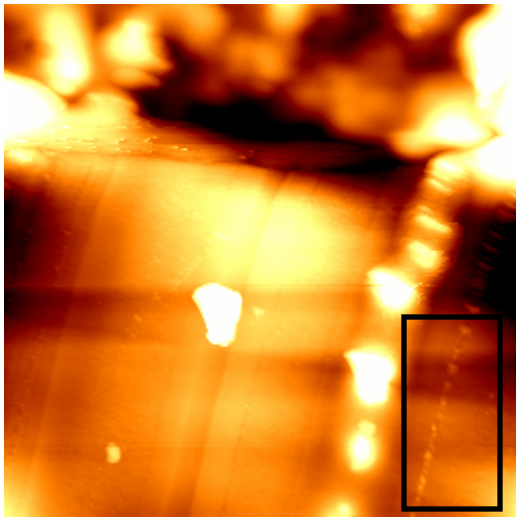

Figure 6 – 25 µm AFM image of TEM sample

Figures 7 through 10 reveal very intricate folds in the polymer. In many of these figures, particles can be seen in channels running perpendicularly to the folds. It is truly difficult to ascertain to what degree the folds and the particle ordering in this image are the result of preparation of the TEM samples and to what degree they are a result of the self-assembling of the ionic liquid material.

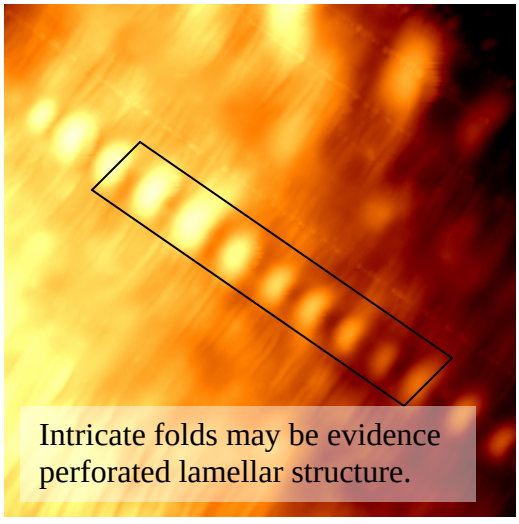

Figure 7 – 25 µm AFM image of TEM sample

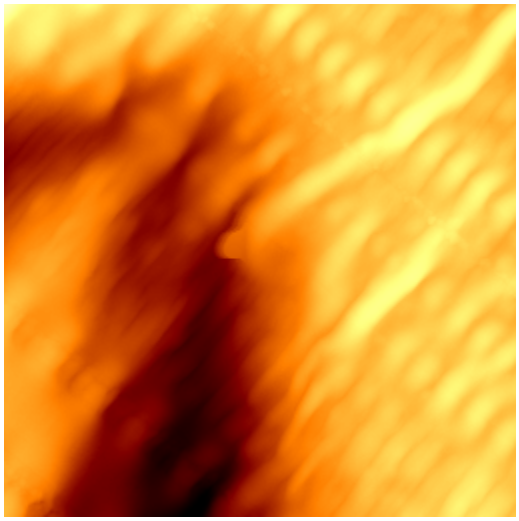

Figure 8 – 25 µm AFM image of TEM sample

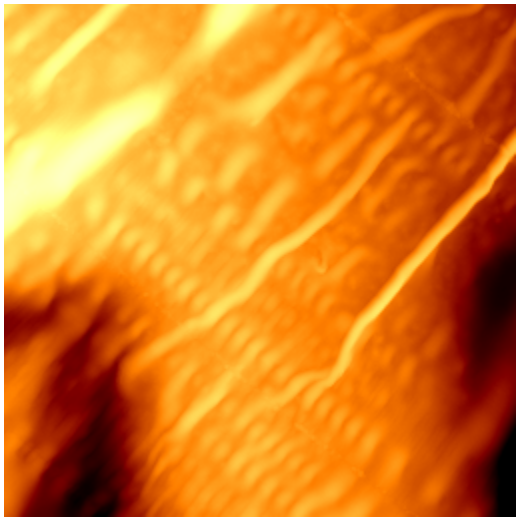

Figure 9 - 45 µm AFM image of TEM sample

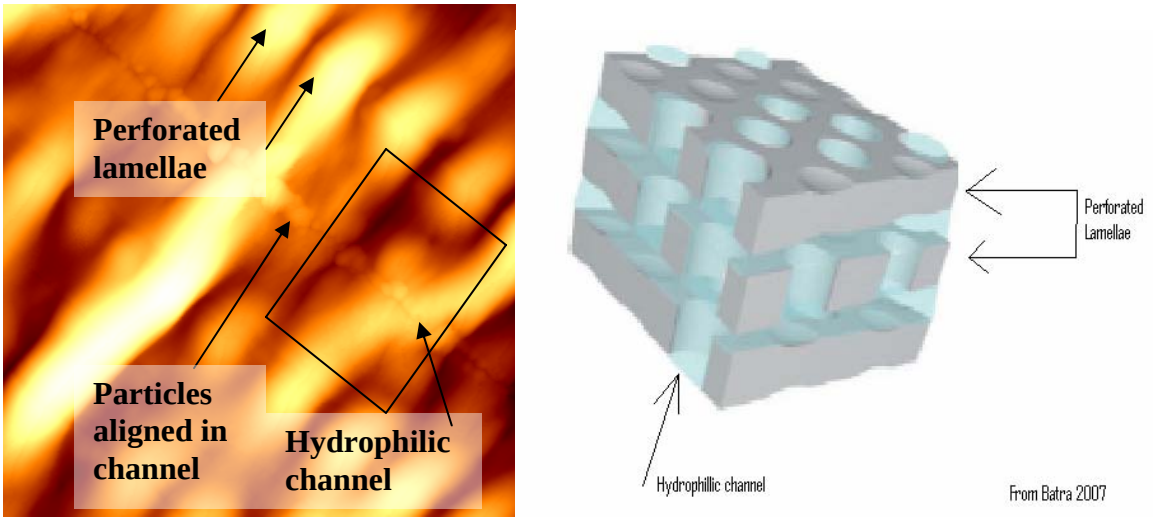

Figure 11 – 10 μm AFM image of TEM sample with Figure 1 for contrast

The overall structure of the polymer in Figures 7 through 10 reflect the self-assembled structure anticipated from previous works. In Figure 1, a schematic of a perforated lamellar structure was depicted. Figure 10 shows what could potentially be the physical form of this structure. The images suggest that there is a stacking of lamellar sheets along one axis, in a series of linear folds. The sizes of the nanoparticles in the previous images range from 200 to 750 nm. These sizes are actually larger than the sizes anticipated from previous works, which implies that they may not be the intended gold nanoparticles, but debris from microtoming (Batra 2007).

Because of the very fine and intricate linearity of these folds and particles, it is possible that the perceived order is the product of sample preparations. Figure 11 shows one intersection of the base grid, upon which the TEM sample rests. In the area scanned, there is a large tear in the sample, which may likely be the result of a sweep by the AFM cantilever. In this image, the very edge of the TEM sample can be seen. Creases at the very edge of the sample follow along the same axis as the folds and particles. It is possible that these creases and the parallel folds could all be the result of the preparation

of the sample and the TEM imaging process. Further investigation of other polymeric samples was necessary in order to draw conclusions about the self-assembling and ordering of the composite structure.

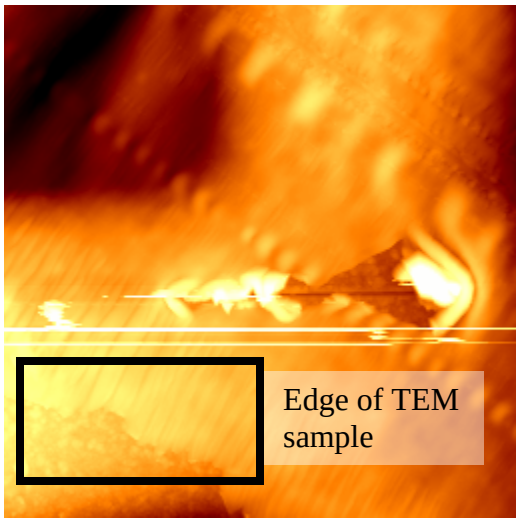

Figure 11 – 45 µm AFM image of TEM sample

A few conclusions may be drawn from figures 6 through 11. While the particles may arrange themselves into linear channels, it is highly unlikely that they reach the degree of linearity seen in the TEM sample images. The folds and particles in the figures above are too uniform and linear to be created solely from a self-assembling polymer. The expected 3D bicontinuous structures and 2D hexagonal packed lamellar structures would occur in near random blocks throughout the polymer and not in order parallel lines across a given sample. Additionally, the particles sizes from these images are not representative of the particle size and packing structure anticipated from the x-ray and IR tests. The TEM samples do not provide enough information to conclude whether or not hydrophilic channels are forming in the polymer.

VI. NON-IMMERSED SAMPLES

The first order of business in investigating the polymeric composites was to determine the distribution and placement of particles within the polymer. This was important simply for the purpose of finding the particles and knowing where to look when searching for self-assembled polymeric structures. As mentioned before, the particles were not evenly distributed throughout the polymeric sample. Therefore, AFM images of the non-immersed samples were taken from one edge of the polymer, where it was obvious that no particles would exist, through the center, to another edge of the sample where particles were very likely. The following images illustrate the progression of these images across the sample.

In Figure 12, jagged contours combined with other wise smooth surfaces can be observed in the scanned regions. This image and the following images were scanned from the cross section of a non-immersed sample which was developed by simply snapping the polymeric cylinder to expose a face to scan (actual sample shown in Figure 2). The jagged contours are likely the result of the tearing necessary to create the polymer sample. These rigid contours are most likely caused by breaking of ordered polymeric structures. Figure 12 was taken near the edge of the non-immersed sample in a

beige colored region where it was highly unlikely that particles were present. Clearly, particles are not present in the area scanned. Besides the jagged features, the surface is relatively smooth. Since no ethanol immersion or drying has occurred, no self-assembly has taken place.

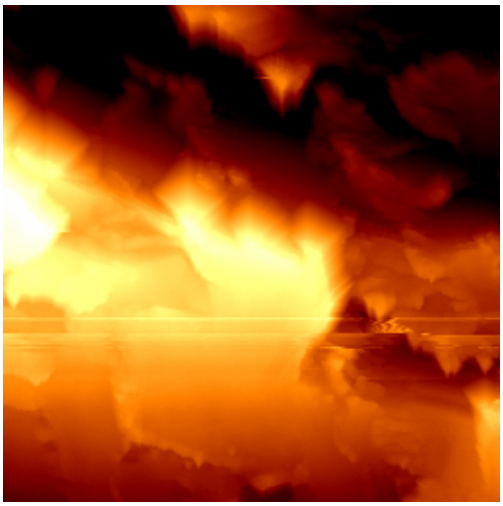

Figure 12 - 20 µm image of beige edge region of non-immersed polymer

It is important to note here that one of the difficulties with imaging a polymeric cross section such as the ones illustrated in the previous and ensuing images is finding an area to scan. Polymeric-gel surfaces typically have very irregular contours. Damage can be incurred to the sweeping cantilever if a particular region has severe regularities in height. If an area is being scanned, and there is a steep increase in height of the sample in a point or area, the cantilever may become bent, stuck, or break as a result of running into the protrusion. Specifically for gels and polymeric type materials, it is possible for the material to get stuck to the AFM cantilever. This causes an increase in tip diameter which affects the accuracy of the captured contours. For Figure 12 and the following figures of sample cross sections, determining what areas would be scanned on the

polymeric-gel was often a function of what regions were possible to scan rather than picking specific regions independently of texture.

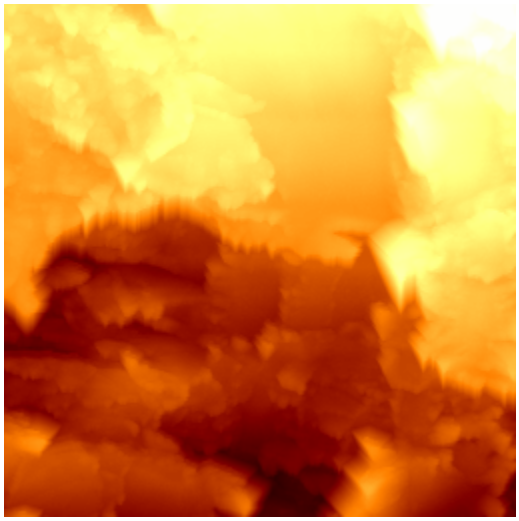

Figure 13 - 20 µm image of beige central-edge region of non-immersed polymer

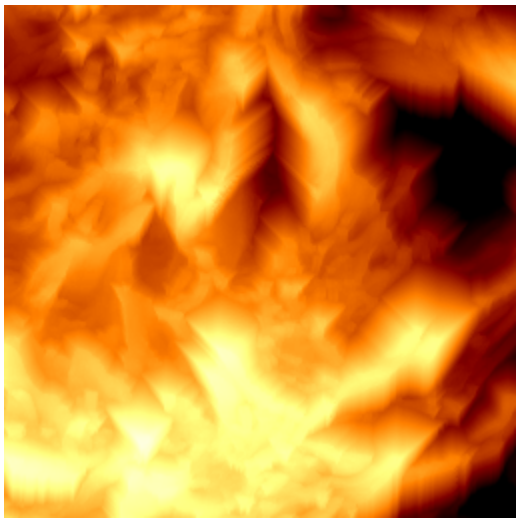

Figure 14 - 20 µm image of central region of non-immersed polymer

Figure 13 and 14 were taken from more central regions of the polymer. The only major changes in terms of structure are that the jagged contours are even more apparent. Again, this sample forms the face of one region torn from the dry, non-immersed gel provided by Argonne. The rigid contours are likely the result of internal, block like structures that break apart during the tearing of the polymer. Once again, these images also possess no

particle or particle-like structures. If particles were present in this region of the sample, they would show up in within the rigid contours of the sample and be widely distributed. Tearing of the polymer did not appear to have an effect on the presence of particles, since the particles are present in the next few images of the same sample. If the particles existed in the central region of the polymer, they would, indeed, show up in the AFM image.

Finally, the dark purple opposite edge of the polymer was examined. Figure 15 illustrates, not only that particles are present in the very edge regions of the composite's cross section, but also that the particles are highly concentrated in this region. This implies either that the particles are not well distributed for some reason during the polymerization reaction, or that the high energy curved surface of the glass tube plays a significant role in the nucleation of the gold nanoparticles. Also, it cannot be said that these are simply dust particles or dirt that has reached the sample. The sample was enclosed during the entire time in which Figures 12 through 15 were taken. Any dirt or dust seen on this edge of the sample should have been evenly distributed over the entirety of the sample and seen in previous images. Additionally, this image was taken after the more jagged images were taken. So it cannot be said that the cantilever was not functioning properly during the image shown in Figure 15, while Figures 12 through 14 were the products of a damaged tip.

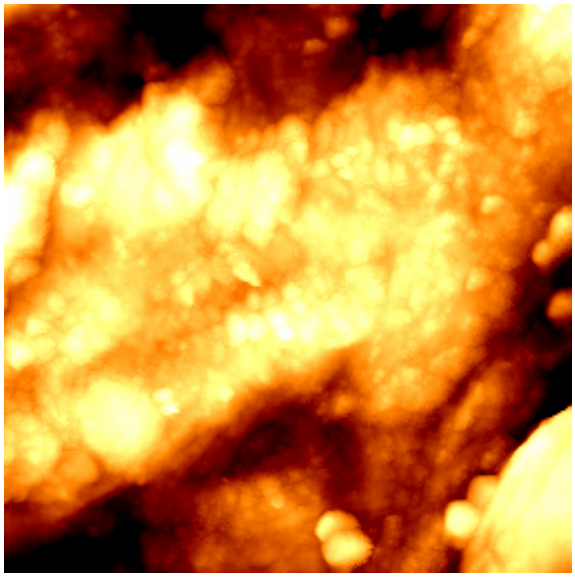

Figure 15 - 10 µm edge of sample in purple region

The particle sizes for the regions scanned in Figure 15 ranged from 100 to 350 nm, which is larger than particles sizes anticipated from previous work. This could however, point to particle agglomeration during nucleation. Also, the particles could be encapsulated in the polymer itself, which would make the particles appear wider due to a polymeric coating. Furthermore, operating the AFM in non-contact mode could add another layer of "thickness" to the particles because the AFM is sensing atomic forces about 100 nm from the physical surface of the sample. These added dimensions may make the particles seem wider than they actually are, which explains the discrepancy between SAXS images from previous works and the current AFM images. Due to the absence of any other particle-like structures anywhere else on this sample, it is unlikely that these particles are anything but agglomerated gold nanoparticles. The distribution of the particles follows expectations. The particles are in high concentrations and in no particular order. This sample has not been immersed in ethanol and allowed to dry. Therefore, the arrangement of the particles seen in Figure 15 is the arrangement of the

particles post-nucleation. After polymerization and nucleation, one would not expect to have organized channels because the environment of the reaction is not conducive to rearrangement of the particles. The ethanol immersion and subsequent drying are what allow the polymer to expand and to self-assemble into a more ordered stable structure that reflects the anticipated order expected of the gold nanoparticles and polymer composite. Ethanol immersion enables the gold nanoparticles to have some mobility within the polymer for arrangement.

Another interesting observation to note is the lack of jagged contours. The fact that there are not really any jagged contours in this region may imply that the nanoparticles are effecting the overall structuring of the polymer during polymerization. Where the polymer seemed to be forming block like rigid structures where no particles were present, it seems that the presence of the nanoparticles cause more globular-spherical structures and contours to form. It is very likely that the gold nanoparticles impede the formation of the rigid polymeric structures seen toward the center of the sample.

Since it was determined that the highest concentrations of particles was exhibited on the very edge of the polymeric sample, images of the side of the polymer, perpendicular to the cross section were investigated. If the glass tube surface in which the material was polymerized was actually nucleating the particles, then the highest concentrations of particles would be seen on the very sides of the polymer in areas where the UV light struck the sample. Figures 16 and 17 show that this was, indeed, the case.

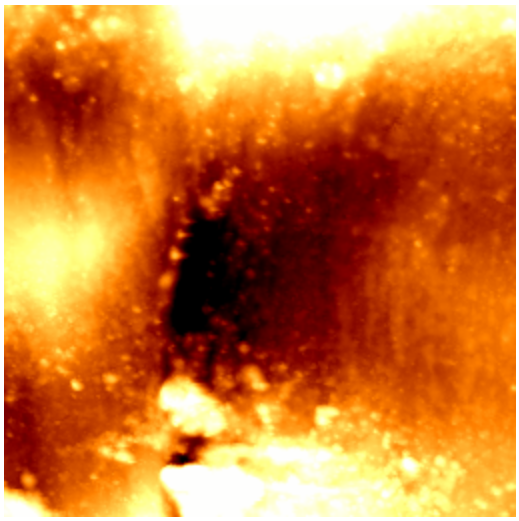

Figure 16 - 20 μm image of purple side of long polymer (not cross-section)

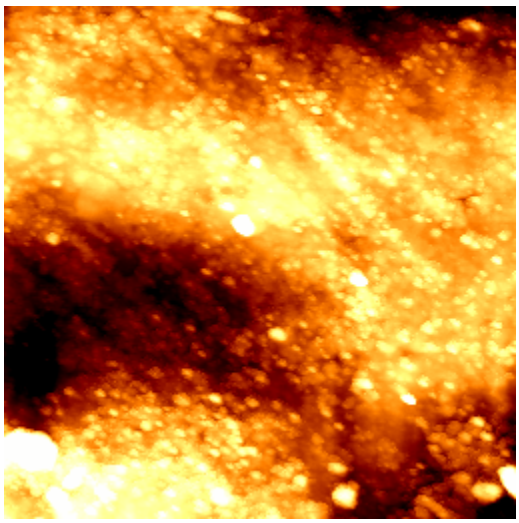

Figure 17 - 6.07 um image of purple side of long polymer (not cross-section)

Clearly, the highest concentration of particles occurs along the sides of the polymeric cylinders. This strongly suggests that the nucleation of the polymer is significantly focused at the surface of the glass tube, or else, once again, the particles are not uniformly distributed in the initial fluid previous to polymerization. The particles are indeed gold as they reflect the expected size of the gold, assuming some agglomeration and inaccuracies due to the nature of AFM imaging. The size of the particles in Figure 17 ranged from 50 to 350 nm. Also, this sample was stored and imaged under the same

conditions as the cross sectional images taken in Figures 12 through 15 above, therefore it cannot be said that the particles present in these images are simply high concentrations of dust or dirt. If this were the case, at least similar concentrations of dust and dirt would appear in all regions of the cross sectional images, but that was not the case. Additionally, dust would also be much larger than the particles. Clearly, these are gold nanoparticles.

VII. IMMERSED SAMPLES

The observations recorded for the non-immersed polymeric samples form an excellent basis from which to contrast the samples which were immersed in ethanol and subsequently dried. The particle size, structure of the polymer, and nanoparticle arrangement change dramatically in contrast to the non-immersed polymeric sample. Where the structure of the non-immersed samples, with the exception of the particle regions, was homogeneous and continuous, the structure of the immersed particles will show porous regions, channel development, particle encapsulation and other important features.

The non-immersed samples that were examined were predominantly those provided by Argonne. These immersed samples were polymerized, immersed in ethanol for three hours, dried for roughly two hours, and then sliced by a fine razor blade, which did not leave any striations. Given that the samples were expanded by ethanol and then dried, the hexagonal packing structures and gold nanoparticles lining the hydrophilic channels of the polymer were expected to develop. A large number of AFM images were created using these particular samples to determine the structure of the polymer resulting from ethanol expansion and drying contraction. Despite the assembly processes induced by ethanol absorption, gold nanoparticles continued to occupy the very edge regions of the polymer. One would expect that the ethanol and subsequent expansion of the

polymer would enable mobility of the nanoparticles, but one would not expect this to imply that the particles would expand to uniform distribution throughout the polymer. Mobility of the particles is increased, but the polymer does not become fluid.

Unlike the surface of the non-immersed samples, it was difficult to take AFM images across the diameter of the samples. This is a result of the shape taken by the sample upon drying. Figure 18 is a schematic of the shape of the dry polymer.

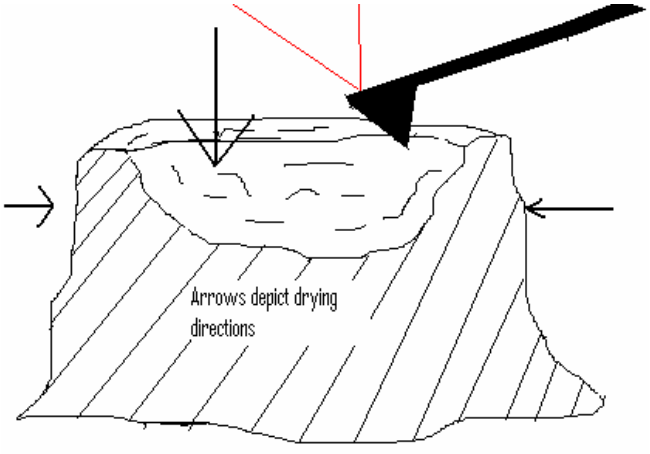

Figure 18 – Schematic of drying immersed sample

During drying, the cylindrical walls of the composite polymer pulled in upon itself. This entailed the walls contracting, and the top face of the sample shrinking in towards the base. The bottom face of the sample, being stuck to Petri dish paper, simply remained stuck while the rest of the sample contracted. The resulting shape of the sample was a bowl-like morphology. The center of the sample was the lowest part of this bowl. Moving away from the center towards the outer boundary, the height of the surface increased parabolically. At the top, outer ridge of the bowl, there were some flat regions, which had enough surface area to perform AFM imaging. Although the sample tended towards a bowl like structure, it was not completely uniform. Much of the time, the higher ridge regions interfered with the cantilever when attempts to take images of the

lower central regions were made. However, there were low ridges where the cantilever could be inserted to take images of the center of the sample. In contrast to the non-immersed sample, where it was relatively simple to take AFM images across the diameter of the sample, more precision was required to image across the immersed samples.

A cursory glance at the immersed polymer composite samples clearly showed that the particles, once again, were located predominantly along the ridge regions of the cylinder. Figure 19 shows that the dark purple regions, which mark the presence of gold nanoparticles, were fixed around the outer edge.

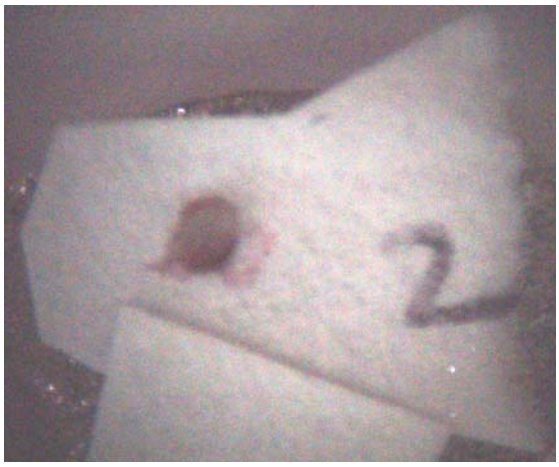

Figure 19 – Cross section of immersed sample

Figure 19 shows the cross sections of the polymeric samples with very dark boundary regions contrasted by more pale central regions. These pale central regions are the result of expansion produced by ethanol. During the expansion the color of the material goes from the beige color, seen in the non-immersed samples, to a pale purple color – except in regions highly concentrated with nanoparticles. Figure 19 seems to show a potential concentration gradient of gold nanoparticles from the purple, center edge of the sample going towards the paler purple center. This may be the case, however, the shape of the

bowl like shape of the surface created during drying made imaging of regions on the slope of the bowl difficult to determine a gradient.

Based on many AFM images generated over the entire surface of these samples, it was found that only the very edge regions of the polymer had any concentration of particles at all. Figures 20 through 23 were taken in the central regions of the polymer and illustrate the fact that the center of the composites are devoid of gold nanoparticles.

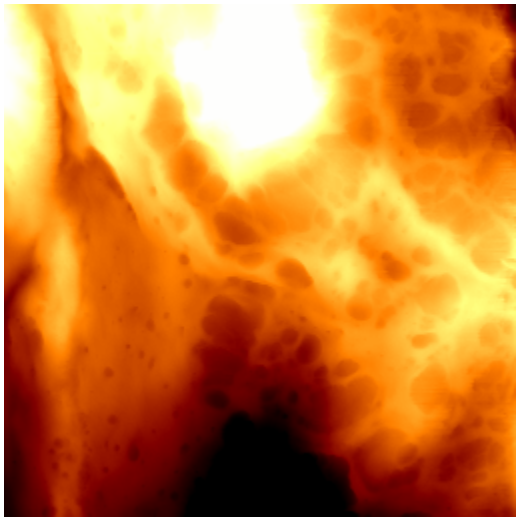

Figure 20 - 20 µm image of the central region of immersed sample 1

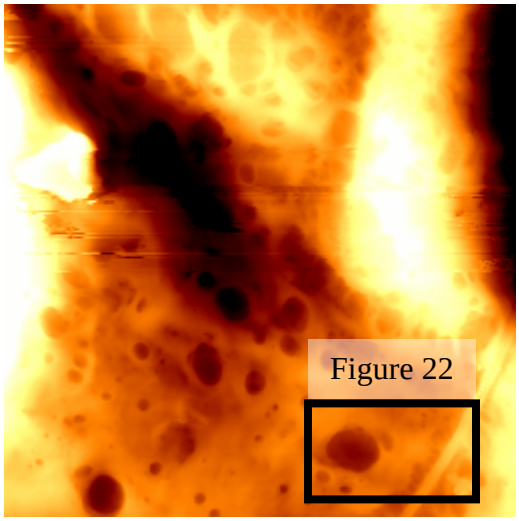

Figure 21 - 15 µm image of the central region of immersed sample 1

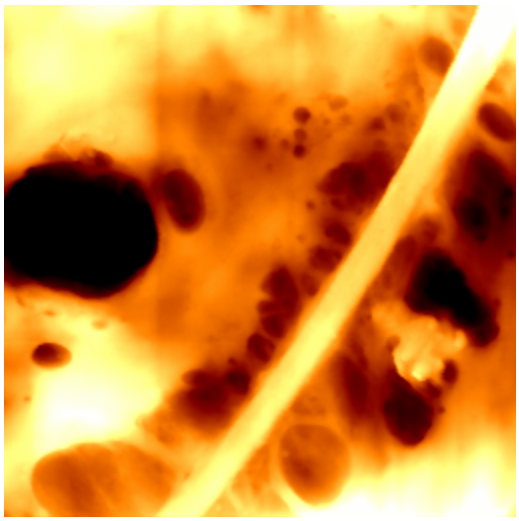

Figure 22 - 4.71 µm image of immersed sample 1

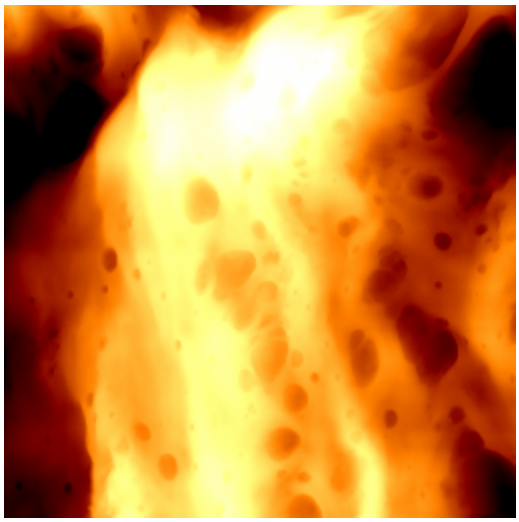

Figure 23 - 10 µm image of immersed sample 2

Figures 20 through 23 reveal features that contrast sharply with the features of the central regions of the non-immersed samples. These immersed sample images depict dendrite like networks and deep pits permeating the composite. These pits and networks are the result of ethanol expansion followed by contraction from ethanol drying. Ethanol is absorbed by the composite polymer upon immersion and expands until the material is fully saturated with ethanol. The provided samples took approximately 3 hours to

become completely swelled with ethanol. Upon contraction from drying ethanol, the hydrophilic bonds between the ethanol and polymer are broken causing the deep pores and dendrite-like networks to form throughout the polymer. In addition to the pores and networks, which form as a result of drying ethanol and contraction of the polymer, other more organized and uniform structures are also formed. This self-assembly is the result of the polymers attempts at creating more favorable stable states. The following images show examples of structural development within the polymer.

Since the regions imaged were completely devoid of particles, gold particles lining channels were not observed. However, empty channels are observable, which gives credence to the idea that the polymer is indeed undergoing structural rearrangements during the drying process and, at times, “organized” structural development.

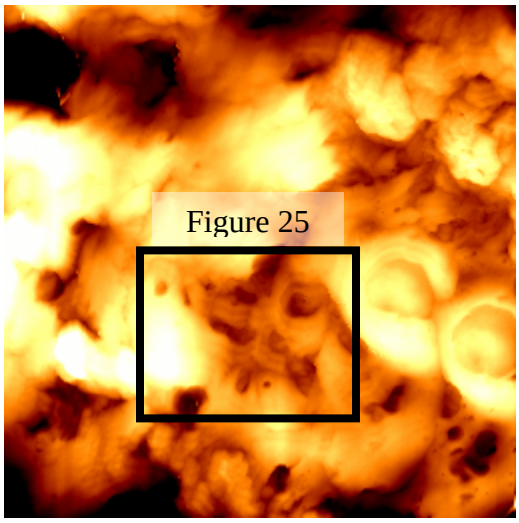

Figure 24 - 20 um, edge of immersed sample 3

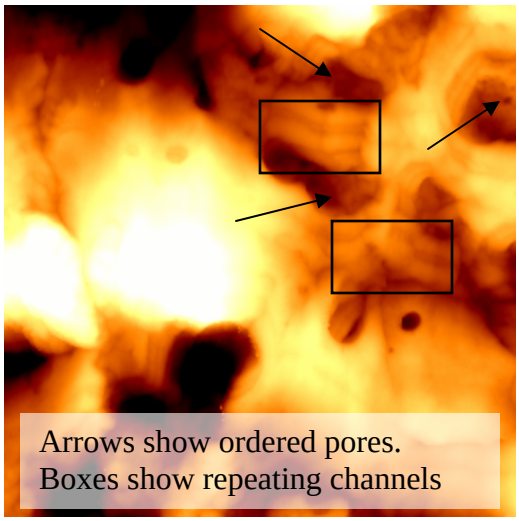

Figure 25 - 7.5 µm image of immersed sample 3

Figures 24 and 25 show, not only pore and network structures, but also more organized, less random characteristics. The top right corner and bottom left corner of Figure 24 show what seem to be layered folds in the polymer. These folds are the packing structures anticipated of the polymer in previous work. Slightly to the right of center in Figure 24 is a cross-like structure, which is more closely imaged in the top right corner of Figure 25. This structure is a more elaborate example of polymeric self-assembly in ionic liquids. Clearly, this structure shows a more intricate order than the simple folds observed around in different regions of these images. Additionally, it is apparent from this image that the assembly of the polymer into different structures at various regions occurs along differing "axes". These multidimensional formations reflect anticipated random ordering of bicontinuous block structures. These structures were anticipated to occur in random blocks, like pockets of order, throughout the polymer as opposed to the entire polymer taking on a uniform order.

It was not until the boundary regions of the immersed composite samples were imaged that the gold nanoparticles began to show up. In contrast to the more internal

regions of the sample, the contours of the boundary region were more diverse in terms of the structure of the polymer. Where the central region seemed to have dendrite type structures and pits, the boundary regions showed smooth surfaces, globular structures, folds lined with particles, scattered particles, and rigid block-like formations. It is very likely that the gold nanoparticles contributed significantly to the formation of these structures, but it is also likely that the crystal wall of the test tube in which the polymer was created may have acted as a foundation for more rigid structures in the boundary regions. Away from the "foundation" of the wall, the polymer may have been more free to assemble itself into the neural-like networks and channels observed in the central region of the sample. The following figures illustrate the varying arrays of actual dimensions in the boundary regions of the polymers.

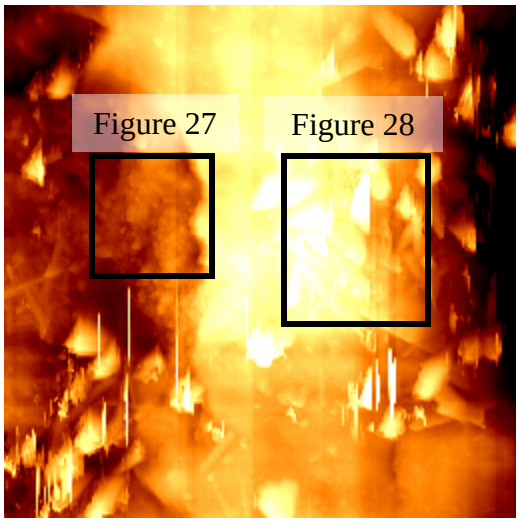

Figure 26 - 20 µm image of immersed polymer edge

Figure 26 is a good example of the diverse array of textures and contours that can be seen in the upper ridge regions of the composite. The central to right hand region of the 20 µm image seems to have a relatively smooth surface with multiple sharp and block like

projections extending through the surface, and some debris looking materials laying on the surface. On the left hand side of Figure 26, more globular and particle-like structures can be observed, in addition to the some of the block like projections largely observed on the right hand side. Closer images of this area are provided in the following figures.

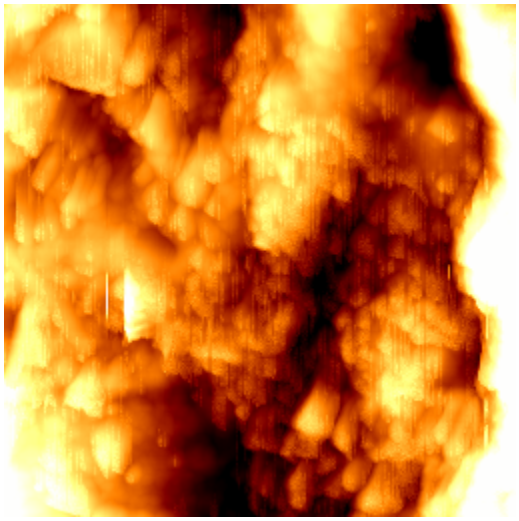

Figure 27 - 6.13 µm image of immersed polymer edge

Figure 28 – 10 µm image of immersed polymer edge

Figure 27 is a closer image of the left hand, central region of Figure 26. Not only are there globular, particle like structures in this particular area, but there are also rod and block like projections as well. Figure 28 is a 10 µm image of the central-right hand side of Figure 26. Large plate and block structures are observable, as well as very rigid protrusions extending through the surface. Upon closer examination, more particulate like characteristics are also revealed. Figures 26 through 28 severely contrast with the relatively smooth and dendrite-like structures of the interior regions of the polymer. One might argue that the irregularities seen here are the result of debris on the sample. While this is a possibility, the following two images were taken from the same sample, with the same tip, in the same session as the images above, yet reveal no debris and a relatively smooth surface. These two images were taken from the central region of the sample. If there were any debris on the sample, one would think that the debris would show up at least somewhat uniformly over the whole sample. Overall, the central region imaged in Figure 29 and 30 is shown to be relatively smooth and free of debris.

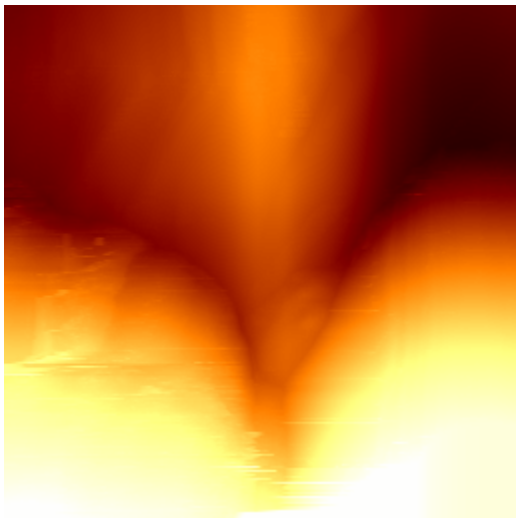

Figure 29 - 10 µm image central region of immersed polymer

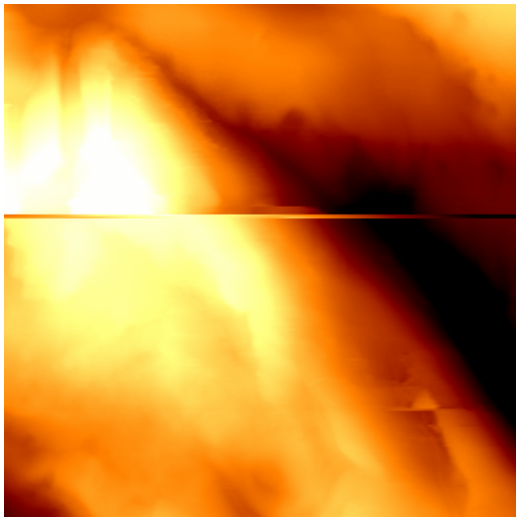

Figure 30 - 10 μm image of central region of immersed polymer

The very sharp projections, the strong rigid surface, and the globular particle structures seen on the ridge regions severely contrast with the smooth, dendrite-like, almost fluid type formations seen in the central regions. It is possible that the gold nanoparticles aid in the rigidity of the structure as well as many of the different formations observed on the polymer in particle populated regions. It is also possible that the rigidity of the polymer in these regions may be a function of how close these regions were to the glass tube wall in which polymerization occurred. The glass tube may have formed a sort of "foundation" for more rigid qualities along the walls of the polymer. The combination of particles and glass wall may completely explain the more rigid structure observed along the ridges of the polymer, which seem to completely lack the more fluid aspects found in the central regions of the polymer. Most likely, the multidimensional drying of the polymer causes the ridge regions to be more densely packed with material than the central regions. For this reason, the contours of the edges of the polymer are more rigid and compact.

The dark purple colored ridge regions of the polymer exhibited a diverse array of textures and characteristics. The composite also showed that relatively organized structures, each with different features, existed along different axis of the polymer. This lends evidence to the idea of 2D hexagonal and 3D bicontinuous structures being formed throughout the volume of the polymer along differing axis.

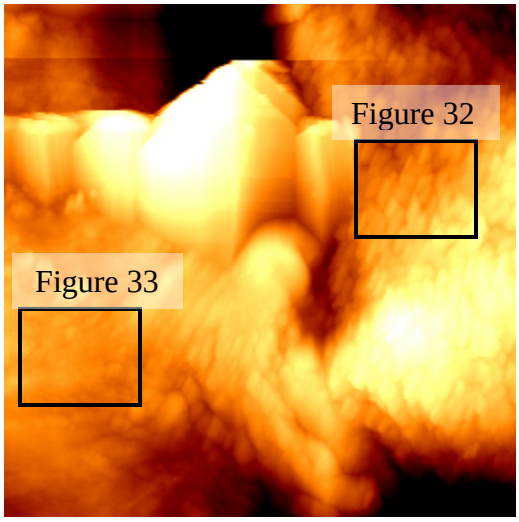

Figure 31 - 20 µm image of non-immersed edge

Figure 31 shows a diverse array of features extending in different directions throughout the entire imaged region. In the lower left hand side, just below the large block-like features, parallel folds are observed extending back into the image. In the central and upper right hand side, up to the top of the image, small, stacked rectangular prism-shaped structures are seen oriented towards a different axis. The large-block like features observed in the upper central region of the image are the result of the AFM cantilever sweeping over a region where the cantilever tip may not reach to, resulting in a large block like structure. If the AFM cantilever could have been turned to a different angle, these blocks may have showed more detailed features. However, these block type features also give credence to the idea that the polymer, upon drying, is creating

relatively ordered features along different axis. The figures below provide some up close detail of Figure 31, to illustrate the ordered nature of the observed features.

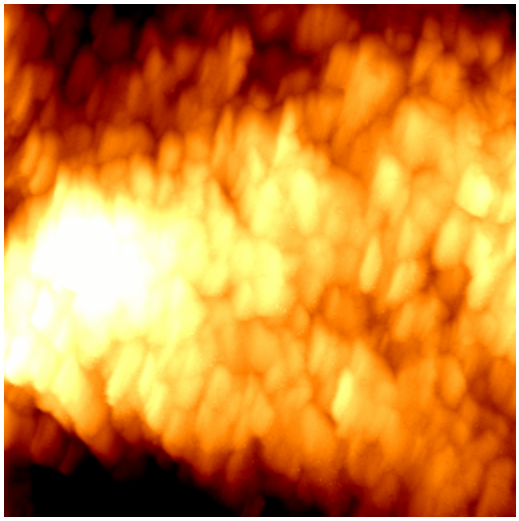

Figure 32 - 9.87 µm image of right hand side of FIGURE 29

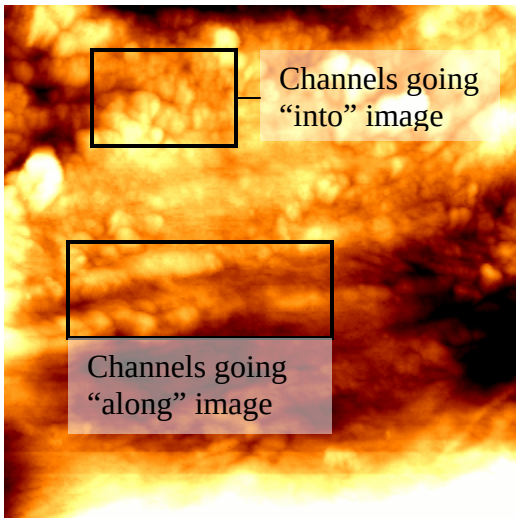

Figure 33- 13.96 µm image of left hand side of FIGURE 29

Figure 32 is an image of the small, seemingly stacked, rectangular prism-shaped structures arranged along a vertical axis and parallel to each adjacent stack. Figure 33 is a 13.96 µm image of the bottom left hand side of Figure 31. In this image, globular, particle features are seen lining parallel rows across the area scanned. It is difficult to

ascertain whether or not these particles are lining any sort of channels in the polymer, or whether or not they are in any sort of packing arrangement. However, this image does illustrate, again, that the polymer and the gold nanoparticles have assembled themselves, upon drying, into a more stable, relatively ordered arrangement in some regions of the polymer.

While some of these images reflect, to some degree, the polymer reorganizing itself during drying, it seems that much of the nanoparticles are sporadically dispersed and highly concentrated throughout the edge regions of the polymer. This could be due to the fact that the nanoparticles are probably nucleating on the wall of the glass test tubes and not capable of moving much further from the wall in order to self-assemble into channel-like structures.

Despite the diversity of surface features, which seem relatively ordered, but not highly ordered, there is evidence that the gold nanoparticles are self-assembling into hydrophilic channels of 2D hexagonally structured regions of the polymer. Figures 34 through 35 depict this evidence.

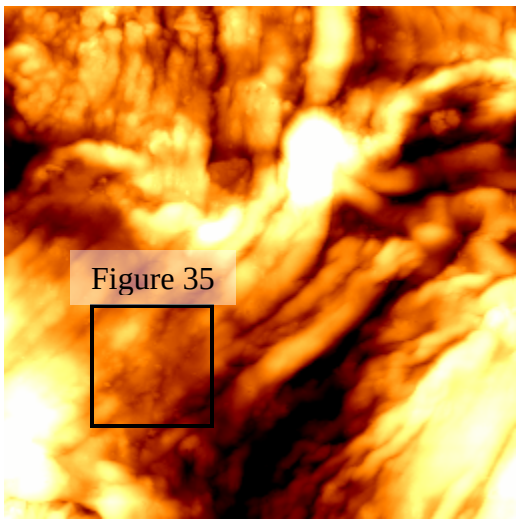

Figure 34 - 20 μm image of immersed sample ridge regions

Figure 34 shows a large quantity of polymeric folds extending in different directions along the axis scanned. Close examination of these folds reveals that many of them are lined with particles in parallel along each channel.

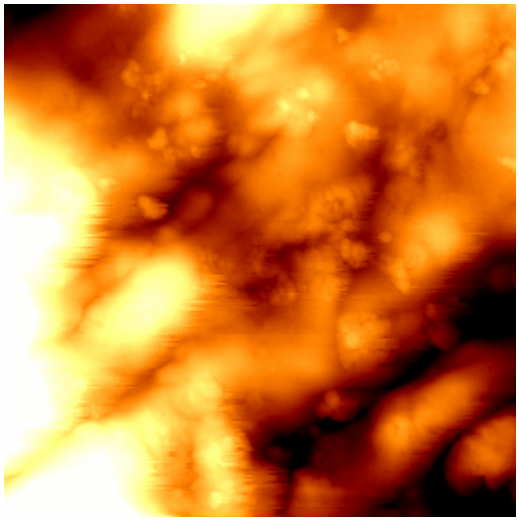

Figure 35 - 4.86 µm site from FIGURE 32

Figure 33, above, is a closer examination of one line of folds from Figure 32. This image shows the polymeric folds in parallel channels across the area scanned. The polymeric channels have gold nanoparticles along the inside of these channels. The particles in Figure 35 range from 100 to 200 nm. This is larger than the sizes anticipated from the SAXS data, but the explanation of this issue in Section VI applies in this situation as well.

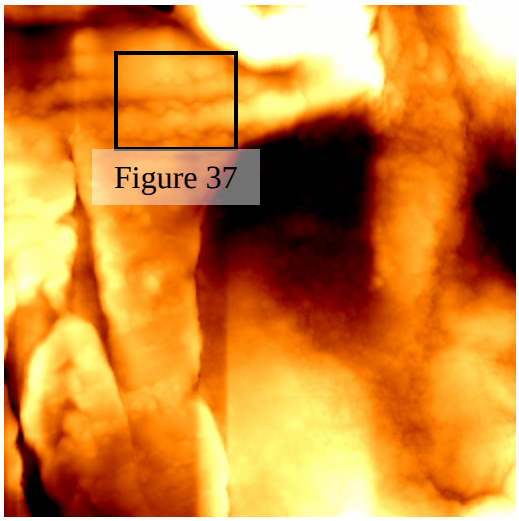

Figure 36 - 20 µm site from immersed sample ridge

Figure 36 is depicts even more ordered hydrophilic channels. Once again, polymeric folds, with aligned particle like structures can be observed in some regions of the scanned area. Another feature of this image is that globular-like structures seen at the base and on the right side of the region scanned in no particular order and along different axis. It is the left hand side, flat folded region that shows an apparent ordering of particles.

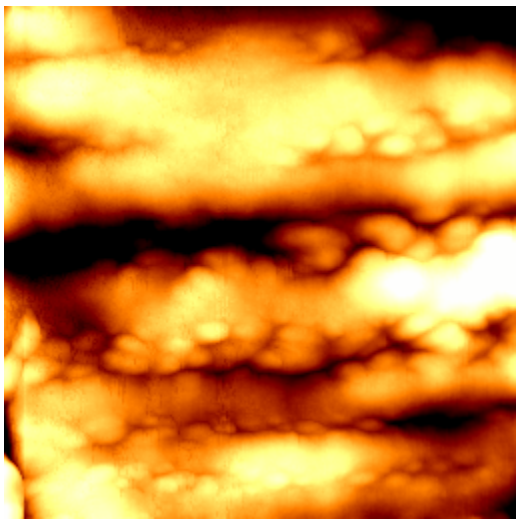

Figure 37 - 5.43 µm site from immersed sample ridge

Figure 37 shows a close up of this region. In contrast to Figure 35, where particles are found in the polymeric folds, but more sporadically, Figure 37 shows a very organized alignment of the particles within parallel channel like regions of the area. The particles in Figure 37 are on the same size range as the particles in Figure 35, however most of the particles tend to be closer to 200 nm in size. The particles observed in this figure take on a more oval shape as well. This is probably the result of more comprehensive encapsulation of the particles by the polymer. The 100 nm to 200 nm size range of particles in Figure 35 correlates to the minor axis of the oval particles. However, when the major axis of the ovular particles is measured the range extends from 100 to 500 nm. Additionally, the arrangement of the particles within these channels is less sporadic and random, in contrast to the particles in Figure 35. In the above image, the particles seem to take on a very ordered stagger stacked arrangement down the length of the polymeric folds. In both Figure 35 and 37, the particles are larger than the anticipated size, but this is a function of AFM imaging and explained in Section VI

The arrangement of particles in these images is not due to high concentrations of particles in certain regions, nor are these merely debris. If the particles were debris, they would not form as organized an arrangement as they do in the two previous figures. Debris would be spread over the area scanned on top of folds or within folds. Clearly, in these images the particles are in high concentrations within the folds. While, indeed, there are some particles spaced sporadically around the area, the highest concentrations are found in the folds. This is evidence for self-assembling nanostructures. If there were no self-assembly the nanoparticles would be in high concentrations but sporadically spaced through the scanned area, independent of fold location. The images assembled

within this work are some of the best examples of polymeric self-assembly. However, because the purpose of the work was to find evidence for these structures specifically, many images were taken of examples of these structures from various samples. The APPENDIX of this work exhibits further examples of these ordered nanoparticle chains within the polymeric channels.

Of high importance in these findings is where these particles are found. As seen before, the polymer exhibits a diverse array of features and structures along different axes of the sample. Images of the nanoparticle laden channels in Figures 34 through 37 can be difficult to obtain because of the guess work involved in choosing sites from which to gather images. Almost all of the gold nanoparticle laden channels found in this work were discovered along the side of the polymer in uniquely angled positions that provide images of the polymer which are not readily available in some regions of the cross-sectional face, nor along the flat side of the polymer. Figure 38 is a drawing of where these channel like features are typically found in the polymer samples.

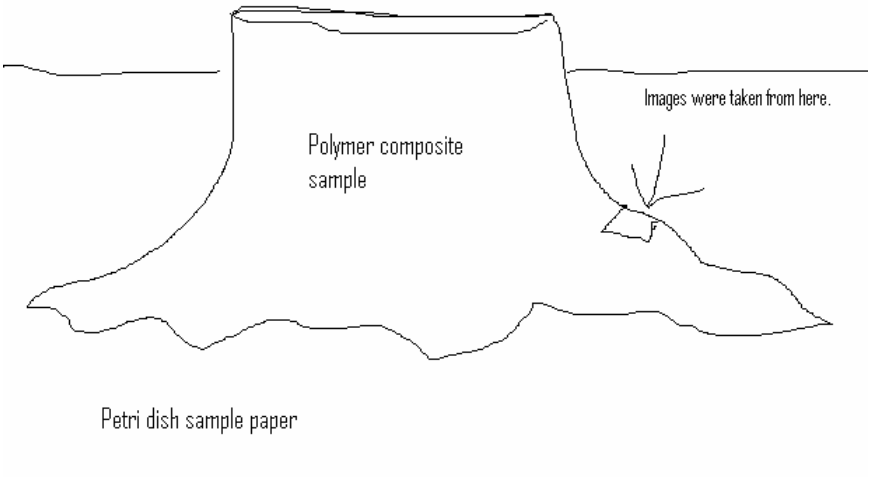

Figure 38 – Diagram of location of channels

The channel-like, particle laden features of the polymer were typically found at the top of regions where the cylindrical sample remained stuck to the Petri dish paper as the rest of the material contracted upon itself. Because of the angle and features created in these regions, sections of the polymer that may not be otherwise observable were brought to light and imaged. Whether or not the features observed in these regions are a product of the unique drying arrangement in these areas, or predominantly the result of polymeric self-assembly is one aspect of this study that could be examined further. Because folds similar to those depicted in Figures 31 and 33 were present in the cross sectional face of the polymer, and because aligned globules and particle-like features are observed elsewhere in the polymer, it is likely that Figures 35 through 37 represent clear examples of hydrophilic gold laden nanoparticle channels and not simply a remnant of the drying process. Because the side regions are more highly concentrated with nanoparticles, it is more likely that the folds created from self-assembly in these regions will be more thoroughly lined with particles then the folds observed in the more "interior" edge regions of the cross sectional face images.

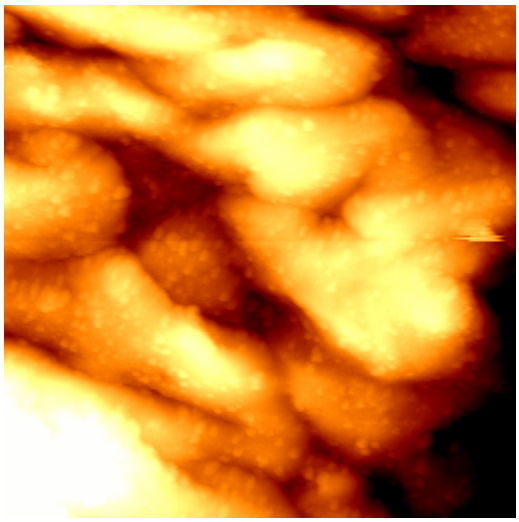

Figure 39 - 20 µm image immersed side

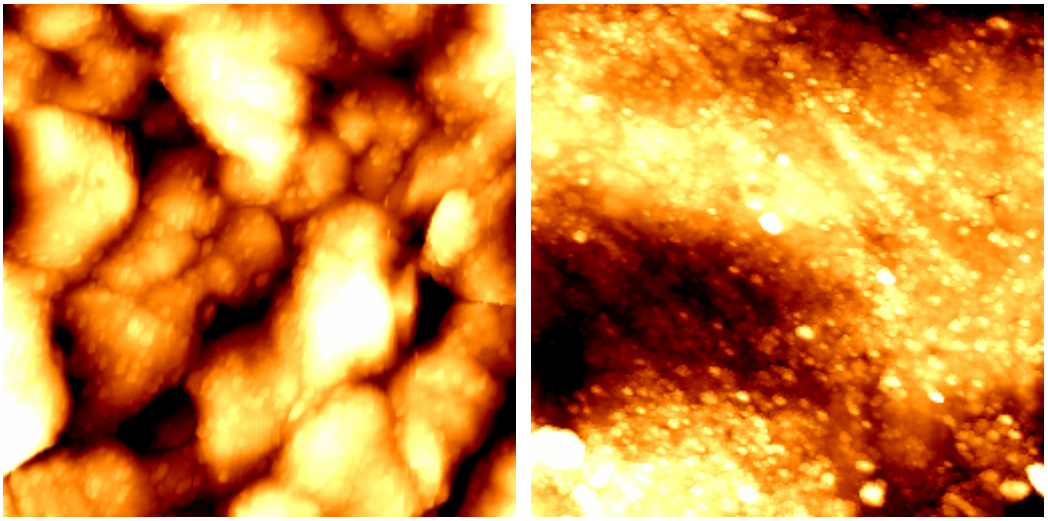

Figure 40 – (left) 25 µm image of immersed side. (right) 6.07 µm image of non-immersed side

In the same way that the cross sectional face features of the immersed polymer severely contrasted with the cross sectional face features of the non-immersed composite, the side regions of the immersed polymer revealed contraction features which contrasted with the non-immersed features. Figure 39 and 40 are images of the side of the immersed polymer samples. The contrast between the immersed and non-immersed samples in terms of side features is striking. Clearly, there is a high degree of rearrangement taking place as ethanol leaves the sample. The images of the non-immersed polymer showed a relatively smooth surface with gold nanoparticles, highly concentrated, and sporadically projecting from the surface of the polymer. In contrast, the immersed sample shows large scale folds and bends in the overall surface of the sample – a result of self-assembly during ethanol drying. The immersed samples also reveal nanoparticles that are more globular and larger in size. In actuality, the larger sized particles are the result of agglomeration and encapsulation by the composite material. The globules seen in Figures 39 and 40 are probably agglomerated gold nanoparticles or thick layering of the polymer around each particle. One may also observe that the distribution of particles

tends towards more even spacing. The large nanoparticles seem to maintain an average uniform distance in spacing for the immersed samples, where as the non-immersed samples were highly populated and tightly packed at the side of the non-immersed composite. It is likely that the very high concentrations of particles in the polymer at the edge regions impedes the ability to assess the overall packing arrangement of the particles along the sides. More work may be needed to see if lower concentrations of particles make finding ordered arrangements simpler. However, it is evident that the polymer is indeed assembling the nanoparticles to a more uniform, energetically preferred state. The order of the state may be a 2D hexagonal structure, but it is difficult to ascertain because the high population of particles do not seem to follow any sort of long-range order. One additional note is that the size of the particles actually appears larger in this particular sample versus the non-immersed sample. This seems to suggest that the presence of and drying of ethanol enables particle mobility to arrangements more stable than the arrangement post-polymerization. The added size may be the result of aggregation of the particles. Previous studies have suggested this phenomenon, and it is verified by the larger, globular like characteristics of the observed particles for this sample, when compared to the smaller, much less globular characteristics of the non-immersed polymer.

VIII. CONCLUSIONS

There are many conclusions that can be drawn from this work. First, it can be concluded that the high energy, glass tube surface plays a very significant role in the nucleation of the gold nanoparticles. Based upon a cursory glance at the sample, one may infer that the reduction of the nanoparticle precursor and nucleation of the nanoparticles is occurring along the glass surface of the capillary tube in which polymerization occurs. The fact that the dark purple regions on the samples, which flag the presence of nanoparticles, are concentrated around the very edge of the samples is a basis for this conjecture. Further examination, with atomic force microscopy, reveals that the polymeric composites are completely devoid of particles across the entirety of their cross section, except on the very edge of the dark purple regions. When AFM was used to image the sides of the provided sample, it was found that the highest concentrations discovered anywhere in the sample were found in the purple strip regions running down the side edge of the polymer. The combined evidence strongly suggests that nucleation of the gold nanoparticles is occurring as a result of contact with the high energy, curved, glass surface of the tube in which polymerization of the material and reduction of the gold nanoparticle precursors occurred.

The next conclusion that can be drawn from this work is that the polymer, during the drying of ethanol from various immersed samples, self-assembles into a more

energetically stable and preferred structure. Figures 20 through 25 illustrate that as ethanol leaves the polymer pores and dendrite-like networks begin to form as a result of broken bonds between the ethanol and hydrophilic sections of the polymer. Figures 24 and 25 reveal ordered structures that arise from the drying process. Figure 25 shows a structure with polymeric folds repeating around particular axes in one region of the polymer. This is strong evidence for self-assembly. Further evidence is seen in images where gold nanoparticles were present in the ridge regions of the immersed samples. Figure 31 is an example of this type of region. Rectangular polymeric prisms can be seen in one section of this image stacked along one axis, with adjacent prisms running parallel to the stacked formations. In another area, on the same image, parallel rows of polymeric channels can be seen running along a different axis. Finally, Figure 33 shows some globular structures arranged in clustered globule formations that seem to exist independently of an axis. This feature is anticipated by previous work and provides evidence that 3D bicontinuous structures are present in random forms throughout the polymer.

AFM images generated on the sides of both the non-immersed and immersed composite samples give further credence to the idea of self-assembly within the polymer. In the non-immersed images, the sides of the polymer are highly concentrated with nanoparticles that are tightly packed along the sides of the sample. However, in the immersed and dried images, globule like structures of agglomerated and encapsulated nanoparticles appear with relatively even spacing between the globules and lower concentrations of particles at the very surface. This strongly suggests particle mobility

and arrangement in the presence of ethanol. Self-assembly is apparent by the uniform distribution and agglomerated arrangement of the nanoparticles in the material.

The purpose of this work was to determine whether or not gold nanoparticles, upon self-assembly of the ionic liquid during the drying of ethanol, were aligning into hydrophilic channels of the hexagonally structured polymers. Evidence from AFM imaging of the polymeric samples has revealed that these arrangements are occurring. Figure 37 depicts channel like folds in the polymer lined with a stagger stacked arrangement of particles. It is very likely that this arrangement is the result of self-assembly because the highest concentrations of particles in the channel like regions of these images lie in the channels themselves. If there were no self-assembly occurring, there would not be a stagger stacked arrangement of particles within the polymer and the particles would be scattered independently of polymeric channels.

The only concern regarding these findings is that the arrangements may be more a function of position in the polymer during drying rather than actually representing an arrangement that is going on within the polymer. Figure 38 shows where the majority of the images of these particle laden channels were taken for different samples. Whether the arrangement of these particles is a function of drying in regions where some of the polymer remains stuck to Petri dish paper while being subsequently pulled in by the remainder of the polymeric column remains to be seen. Further work is necessary to investigate how to optimize the presence of these particle-laden channel formations.

IX. RECOMMENDATIONS FOR FURTHER WORK

The ability to analyze the nanoparticle composite polymers is dependent upon the dimensions of given samples. In this work, a cylindrical composite gel was provide by Argonne scientists. This gel had a high concentration of nanoparticles in thin strips along the outer ridge and side of the polymer. AFM was utilized to analyze the edge of cross sectional regions as well as the sides of the cylinder where high concentrations of particles were present. There are several of variables that can be changed in future work to gain more comprehensive knowledge of the internal dimensions and self-assembled structures of the composite.

Experiments could be conducted where the concentration of the particles is varied to see how the overall self-assembly of the polymer is affected. It was observed that there were high concentrations of particles in the material along the ridge regions. This high concentration, which caused the particles to be tightly packed before the addition of ethanol, may impede particle mobility to some degree. Therefore, polymerizing the composite material with varying degrees of particle concentrations may reveal more self-assembled structures than seen in this work. Instead of the combination of ordered structures, with randomly dispersed particles in many areas, it is thought that fewer particles may enable the polymer to more easily assemble ordered structures alone.

The polymer could be developed in shorter tubes with more uniform distribution of the particles throughout the polymer. A small Petri dish sort of set up may work very well for this. If the precursor was at least uniformly distributed around a short Petri dish and along the bottom, more structural qualities of the polymer could be examined. This would also make imaging of the polymer via AFM easier because the cantilever would not have to scan at odd angles to try and reach a strip of particles. If the particles were more evenly distributed in a thinner more uniform polymer surface, the AFM's cantilever could more readily access particles and structures from a wider variety of angles. Additionally, a uniform distribution of particles, at varying concentrations per sample, may also lend to particle mobility while immersed in ethanol and reveal more well ordered structures.

If the polymer composite were developed in a lens or watch glass, it may be possible to see the effect the particles play on the polymer in a longitudinal type cross section. In the current setup, there is a lot of space in the polymer where no particles are present, which makes it difficult to see what the particles are doing at very small distances from the glass surface. A longitudinal cross section may reveal more structural properties than a "latitudinal" cross section. Also, the bent glass surface would aid in nucleating more particles in a lens type setup.

Finally, it was clear the UV radiation only nucleated gold particles on the very surface of the polymeric sample. Further attempts to provide UV uniformly throughout the material would improve AFM analysis and potentially form more of the desired hydrophilic channel structures.

In short, attempts made to change the geometric shape and size of the polymeric cylindrical samples would be beneficial in terms of providing more regions to analyze via AFM. Attempts made at changing particle distribution and concentration within the sample may lend to improved particle mobility and better development of self-assembled structures in the polymer.

REFERENCES CITED

Adachi, E., *Langmuir* **2000**, *16*, 6460.

Batra, D., S. Seifert, L.Varela, A. Liu, and M. Firestone, *Adv. Funct. Mater*. **2007**, 17, 1279-1287

Hoshino, K., M. Yoshio, T. Mukai, K. Kishimoto, H. Ohno, T. Kato, *J. Polym. Sci., Part A: Polym. Chem.* **2003**, *41*, 3486.

Kato, T., N. Mizoshita, K. Kishimoto, *Angew. Chem. Int. Ed.* **2006**, *45*, 38.

Lee, H., S. H. Choi, T. G. Park, *Macromolecules* **2006**, *39*, 23.

Lin, Y., H. Skaff, T. Emrick, A. D. Dinsmore, T. P. Russell, *Science* **2003**, *299*, 226.

McMillan, R., C. D. Paavola, J. Howard, S. L. Chan, N. J. Zaluzec, J. D. Trent, *Nat. Mater.* **2002**, *1*, 247.

Peceros, K., X. D. Xu, S. R. Bulcock, M. B. Cortie, *J. Phys. Chem. B* **2005**, *109*, 21 516.

Shenhar, R., T. B. Norsten, V. M. Rotello, *Adv. Mater.* **2005**, *17*, 657.

Shenhar, R., T. Norsten, V. Rotello, *Adv. Mater*. **2005**, 17, No. 6, March 22

Warner, M., J. E. Hutchison, *Nat. Mater.* **2003**, *2*, 272.

Yoshizawa, H., T. Mihara, N. Koide, *Liq. Cryst.* **2005**, *32*, 143.

Zehner, R., W. A. Lopes, T. L. Morkved, H. Jaeger, L. R. Sita, *Langmuir* **1998**, *14*, 241.

APPENDIX

Figure 41 - 20 µm image of immersed polymer edge

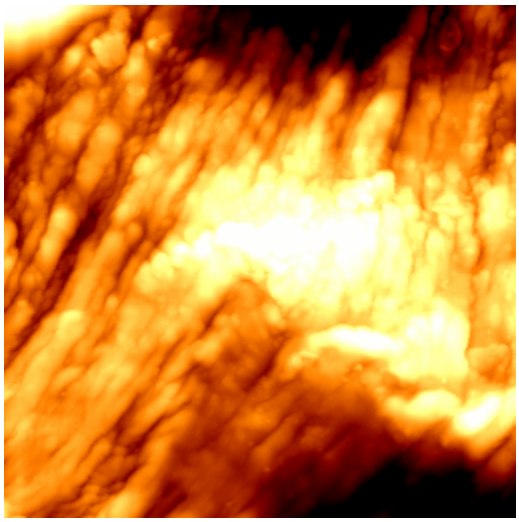

Figure 42 - 7.93 µm image from an area of Figure 40

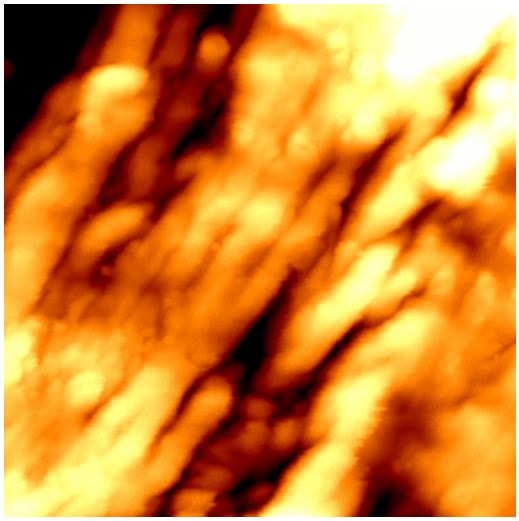

Figure 43 - 2.93 µm image – a closer look at Figure 41